van der Waals theory for solids

A.Daanoun[1], C. F. Tejero[2] and M. Baus[1]
[1]*Faculté des Sciences, Code Postal 231, Université Libre de Bruxelles, B-1050 Brussels, Belgium*
[2]*Facultad de Ciencias Físicas, Universidad Complutense de Madrid, E-28040 Madrid, Spain*
(Received 9 May 1994)

In analogy with the well-known theory for fluids, a van der Waals theory for solids is proposed. It is shown that, in agreement with recent predictions, the competition between the van der Waals loop of the fluid and the van der Waals loop of the solid can produce three different types of phase diagrams for a simple fluid. This could be of relevance to the phase behavior of colloidal dispersions.

PACS number(s): 64.70.Dv, 64.10.+h, 82.70.−y

I. INTRODUCTION

The van der Waals (vdW) theory [1] is remarkable in that, although based on very simple ideas about the intermolecular interactions, it is nevertheless capable of describing the complex behavior associated with the liquid-gas transition, including its critical point, with very simple algebraic means. As such its value cannot be overestimated, not only as a pedagogical tool but also because it did pave the way to the improved vdW-like theories which lie at the heart of our present understanding of the liquid state [2].

Recently it was found, both by simulations [3] and by theory [4], that a vdW loop can develop not only in the fluid phase, as in the original vdW theory, but also in the solid phase. This then suggests that there should be a solid-phase counterpart to the original fluid-phase vdW theory. In the present study, we will introduce such a theory for the vdW loop of the solid and explore its consequences for the phase diagram. The purpose of this study is hence to yield a better understanding of the more exact results of [3,4] and to provide a simple analysis of the phase behavior of colloidal dispersions for which some of these phenomena could be observable.

In the following, we recall the approximations behind the vdW theory (Sec. II) and derive the vdW theory for the fluid (Sec. III) and the solid (Sec. IV) phases. The resulting phase behavior is discussed in Sec. V, while our conclusions are gathered in Sec. VI.

II. THE vdW APPROXIMATION

There are many ways to present the vdW theory. In order to obtain a unified presentation for both the fluid and the solid phases we will start from the Gibbs-Bogoliubov inequality [2] but this is by no means the only way to proceed. The Gibbs-Bogoliubov inequality itself can also be derived in various ways. A short derivation goes as follows. The definition of the Helmholtz free energy F reads

$$-\beta F = \ln \int d\Gamma\, e^{-\beta H(\Gamma)}, \tag{2.1}$$

where $\beta = 1/k_B T$ with T the temperature and k_B Boltzmann's constant, and $H \equiv H(\Gamma)$, the Hamiltonian of our system, is defined over the phase space Γ with $\int d\Gamma\, e^{-\beta H}$ denoting the usual canonical partition function. Let F_0 denote the free energy of a reference system with Hamiltonian $H_0 \equiv H_0(\Gamma)$ defined over the same phase space Γ and related to F_0 by a relation similar to (2.1). Subtracting both relations we obtain, after some rewriting,

$$-\beta(F - F_0) = \ln \langle e^{-\beta(H-H_0)} \rangle_0, \tag{2.2}$$

where $\langle\,\rangle_0$ denotes the canonical average over the reference system. Using the convexity of the logarithm we have

$$\ln \langle e^{-\beta(H-H_0)} \rangle_0 \geq \langle \ln e^{-\beta(H-H_0)} \rangle_0, \tag{2.3}$$

where the right hand side of (2.3) equals $-\beta\langle (H - H_0)\rangle_0$, and combining with (2.2) we obtain

$$F - F_0 \leq \langle (H - H_0)\rangle_0 \tag{2.4}$$

which is the announced Gibbs-Bogoliubov inequality. Equation (2.4) can be rewritten as

$$F \leq F_1 = F_0 + \langle (H - H_0)\rangle_0, \tag{2.5}$$

where F_1 is identical to the first-order expansion of F around F_0. When H and H_0 differ only by the nature of the pair-potential we have for (2.5)

$$F \leq F_1 = F_0 + \frac{1}{2}\int d\mathbf{r}_1 \int d\mathbf{r}_2\, \rho_2^0(\mathbf{r}_1, \mathbf{r}_2)\,[V(r_{12}) - V_0(r_{12})], \tag{2.6}$$

where $r_{12} = |\mathbf{r}_1 - \mathbf{r}_2|$, while $V(r_{12})$ and $V_0(r_{12})$ denote, respectively, the pair potential of the system and of the reference system, and $\rho_2^0(\mathbf{r}_1, \mathbf{r}_2)$ is the pair density of the reference system. The vdW theory is based on taking, as a reference system, a system with purely repulsive forces. To this end we will split the total pair potential, $V = V_R + V_A$, into a repulsive (V_R) and an attractive (V_A) part and take $V_0 \equiv V_R$ so that (2.6) becomes with this choice of reference system:

$$F \leq F_1 = F_R + \frac{1}{2}\int d\mathbf{r}_1 \int d\mathbf{r}_2\, \rho_2^R(\mathbf{r}_1,\mathbf{r}_2)\, V_A(r_{12}), \tag{2.7}$$

where F_R and $\rho_2^R(\mathbf{r}_1,\mathbf{r}_2)$ denote, respectively, the free energy and the pair density of a reference system with purely repulsive forces corresponding to the pair-potential $V_R(r_{12})$. From the exact inequality (2.7) one obtains the vdW theory by introducing three approximations. First, one takes the upper bound F_1 as the estimate of the free energy F:

$$F \simeq F_R + \frac{1}{2}\int d\mathbf{r}_1 \int d\mathbf{r}_2\, \rho_2^R(\mathbf{r}_1,\mathbf{r}_2)\, V_A(r_{12}) \tag{2.8}$$

and, second, one approximates the exact upper bound F_1 by neglecting all the correlations within the domain of $V_A(r_{12})$, i.e.,

$$\int d\mathbf{r}_1 \int d\mathbf{r}_2\, \rho_2^R(\mathbf{r}_1,\mathbf{r}_2)\, V_A(r_{12}) \simeq \int d\mathbf{r}_1 \int d\mathbf{r}_2\, \rho_1^R(\mathbf{r}_1)\, \rho_1^R(\mathbf{r}_2)\, V_A(r_{12}), \tag{2.9}$$

where $\rho_1^R(\mathbf{r})$ is the one-body density of the reference system with $V_R(r)$ as pair potential. Notice that because of (2.9) the vdW theory is a mean-field approximation. The vdW approximation, F_{vdW}, to the exact free energy, F, of a system with the pair potential, $V = V_R + V_A$, reads, thus,

$$F_{vdW} = F_R + \frac{1}{2}\int d\mathbf{r}_1 \int d\mathbf{r}_2\, \rho_1^R(\mathbf{r}_1)\, \rho_1^R(\mathbf{r}_2)\, V_A(r_{12}) \tag{2.10}$$

but for notational facility we will henceforth drop the subscript vdW on F_{vdW}. The final ingredient of the vdW theory, which can be considered as the third approximation, consists in approximating V_R by a simple hard-sphere (HS) potential which leads then to an explicit expression for $F_R \equiv F_{\rm HS}$ when the latter is obtained by thermodynamic integration of a simple HS equation of state. We will thus write the pair potential $V(r)$ henceforth as, $V(r) = \epsilon[\phi_{\rm HS}(x) + \phi_A(x)]$, where $x = r/\sigma$ with σ the HS diameter:

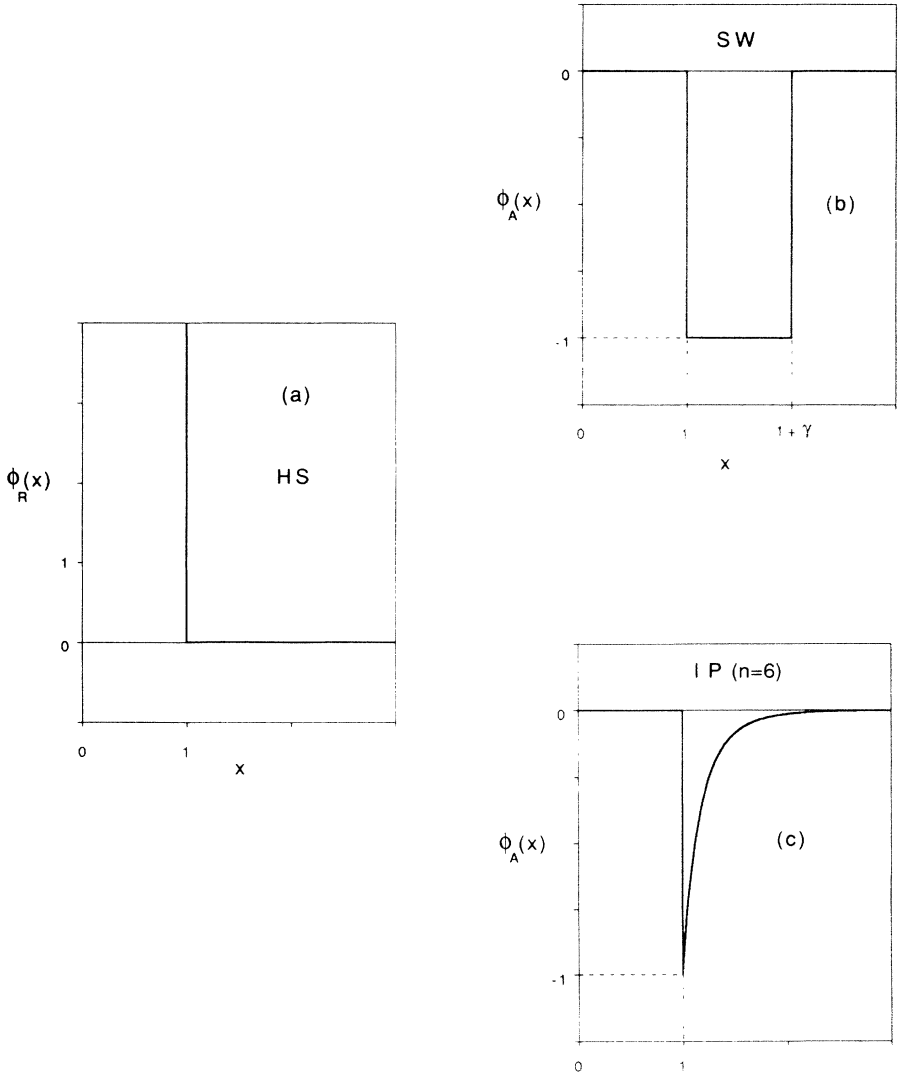

FIG. 1. In the van der Waals (vdW) theory the repulsive part (ϕ_R) of the total pair potential ($\phi_R + \phi_A$) is, as shown in (a), represented by a simple hard-sphere (HS) interaction. For the attractive part (ϕ_A) we will, for the purpose of illustration, consider two cases: (b) a square-well (SW) attraction of range γ, and (c) an inverse-power (IP) attraction of index n [see also (2.11–2.14); the IP potential shown here corresponds to $n = 6$].

$$\phi_{\rm HS}(x) = \begin{cases} \infty, & x \le 1 \\ 0, & x > 1 \end{cases} \tag{2.11}$$

and ϵ the well depth of the attractions described by

$$\phi_A(x) = \begin{cases} 0, & x < 1 \\ -\phi(x), & x \ge 1, \end{cases} \tag{2.12}$$

where $\phi(x) \ge 0$, and $\phi(x)$ tending to zero as x tends to infinity. Below we will moreover illustrate our results with the help of two simple forms of attraction: (a) a square well (SW) of range γ

$$\phi(x) = \begin{cases} 1, & 1 \le x \le 1+\gamma \\ 0, & x > 1+\gamma \end{cases} \tag{2.13}$$

as the prototype of a discontinuous potential, and (b) an inverse power (IP) potential of index n

$$\phi(x) = \frac{1}{x^n}; \quad n > 3 \tag{2.14}$$

as the prototype of a continuous potential (see Fig. 1). Obviously, many other choices are possible.

III. THE vdW THEORY OF THE FLUID PHASE

Although this theory is very well known [1], in order to stress the analogy with the developments of the next section, we briefly repeat the main steps here. For a uniform fluid phase we have

$$\rho_1^{\rm HS}(\mathbf{r}) = \rho, \tag{3.1}$$

where ρ is the number density of the N particles. Using dimensionless free energies per particle, $f = F/N\epsilon$ and $f_{\rm HS} = F_{\rm HS}/N\epsilon$, we rewrite (2.10, 2.11) as

$$f = f_{\rm HS} + \Delta f \tag{3.2}$$

with, on using (3.1) and (2.12),

$$\Delta f = \frac{\rho}{2\epsilon} \int d\mathbf{r}\, V_A(r) = -2\pi\rho\sigma^3 \int_1^\infty dx\, x^2\, \phi(x) \tag{3.3}$$

together with

$$f_{\rm HS} = t\left[\ln(\rho\Lambda^3) - 1 + \int_0^\rho \frac{d\rho'}{\rho'}\left(\frac{\beta p_{\rm HS}(\rho')}{\rho'} - 1\right)\right], \tag{3.4}$$

where $t = k_BT/\epsilon$ is the reduced temperature and Λ the thermal de Broglie wavelength of the HS. From f one can obtain the reduced chemical potential, $\bar\mu = \mu/\epsilon$, and the reduced pressure, $\bar p = p\sigma^3/\epsilon$, from

$$\bar\mu = \frac{\partial(\rho f)}{\partial\rho}; \quad \bar p = -\frac{\partial f}{\partial v}, \tag{3.5}$$

where $v = 1/\rho\sigma^3$. We recall also that (3.4) is nothing but the exact relation between the (HS) free energy and the (HS) equation of state or compressibility factor $(\beta p_{\rm HS}/\rho)$, which results from integrating the pressure equation of (3.5) along an isotherm. As usual in the vdW theory, $f_{\rm HS}$ will be prescribed by adopting an equation of state for the HS. For the latter we take a simple free-volume approximation:

$$\frac{\beta p_{\rm HS}(\rho)}{\rho} = \frac{1}{1-\eta}; \quad \eta < 1 \tag{3.6}$$

so that $(1-\eta)V$ is the average volume freely accessible to the HS in a fluid of volume V. We write $\eta = \rho/\rho_0$, so that ρ_0 is the maximum density ($\rho < \rho_0$) for which the HS fluid can exist. The precise value of ρ_0 is immaterial here but will be discussed further in Sec. V. Notice that the standard vdW theory follows only when taking $\rho_0 = 6/\pi\sigma^3$, in which case η is the packing fraction. Using (3.6), Eq. (3.4) can be easily integrated yielding for (3.2) and (3.5):

$$f = t\left[C_f + \ln\frac{\eta}{1-\eta}\right] - \eta\Gamma, \tag{3.7}$$

$$\bar\mu = t\left[C_f + \ln\frac{\eta}{1-\eta} + \frac{1}{1-\eta}\right] - 2\eta\Gamma, \tag{3.8}$$

$$\frac{\bar p}{\rho_0\sigma^3} = \frac{t\eta}{1-\eta} - \eta^2\Gamma, \tag{3.9}$$

where

$$C_f = \ln(\rho_0\Lambda^3) - 1; \quad \Gamma = 2\pi\rho_0\sigma^3 \int_1^\infty dx\, x^2\, \phi(x), \tag{3.10}$$

or

$$\Gamma_{\rm SW} = \frac{2}{3}\pi\rho_0\sigma^3[(1+\gamma)^3 - 1] = 2\pi\rho_0\sigma^3\gamma\left(1 + \gamma + \frac{1}{3}\gamma^2\right), \tag{3.11a}$$

$$\Gamma_{\rm IP} = \frac{2\pi\rho_0\sigma^3}{n-3} = 2\pi\rho_0\sigma^3\frac{1}{n}\left(\frac{1}{1-\frac{3}{n}}\right), \tag{3.11b}$$

for, respectively, a SW attraction (a) of range γ, and an IP attraction (b) of index n ($n > 3$). It is also seen from (3.11) that for attractions of short range ($\gamma << 1$ or $n >> 1$) $1/n$ plays the same role as γ. The consequences of the vdW theory embodied in (3.7–3.9) are well known. The form of (3.7) leads to a vdW loop. To obtain the corresponding critical point (η_c, t_c, p_c) one solves

$$\frac{\partial\bar p}{\partial\eta} = 0; \quad \frac{\partial^2\bar p}{\partial\eta^2} = 0, \tag{3.12}$$

which yields on using (3.9)

$$\eta_c = \frac{1}{3}, t_c = \frac{8}{27}\Gamma, \frac{p_c}{\epsilon\rho_0} = \frac{1}{27}\Gamma. \tag{3.13}$$

The complete fluid(F_1)-fluid(F_2) coexistence curve can also be obtained by solving the two-phase coexistence conditions:

$$\bar{p}(\eta_1, t) = \bar{p}(\eta_2, t), \tag{3.14a}$$

$$\bar{\mu}(\eta_1, t) = \bar{\mu}(\eta_2, t), \tag{3.14b}$$

where η_1 denotes the value of η for the low-density fluid phase F_1, and η_2 that of the high-density fluid phase F_2. From (3.8,3.9) we obtain for (3.14)

$$(\eta_1 + \eta_2)(1 - \eta_1)(1 - \eta_2) = \frac{8}{27}\frac{t}{t_c}, \tag{3.15a}$$

$$\ln \frac{\eta_2(1 - \eta_1)}{\eta_1(1 - \eta_2)} = \frac{27}{8}\frac{t_c}{t}(\eta_2 - \eta_1)(2 - \eta_1 - \eta_2), \tag{3.15b}$$

which since (3.15) depends only on t/t_c and η/η_c embodies a law of corresponding states, leading to the universal coexistence curves in the $t - \eta$ and $p - t$ planes shown in Fig. 2. Notice also that the law of rectilinear diameters which states that the midpoints of the coexisting densities lie on a straight line in the $t - \eta$ diagram [5], $\eta_1 + \eta_2 \simeq 2t/3t_c$, although very well satisfied near the critical point (see Fig. 2) is not an exact property of (3.15).

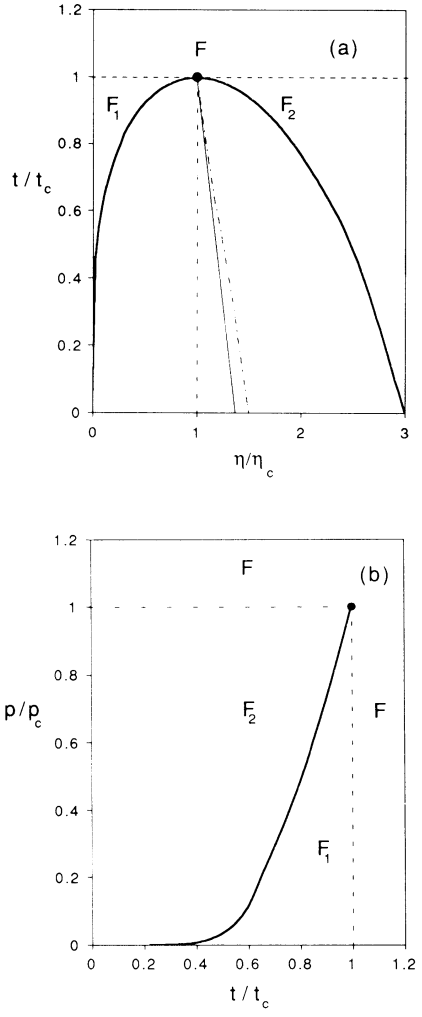

FIG. 2. The universal coexistence curves in (a) the temperature(t)-density(η) and (b) the pressure ($\bar{p}$)-temperature(t) planes for the fluid(F_1)- fluid(F_2) coexistence as obtained from the vdW free energy (3.7). Here F_1 denotes the low-density fluid (or gas) and F_2 the high-density fluid (or liquid) phase in which the fluid phase F separates for temperatures below the critical temperature. All quantitities are refered to their critical point (full dot) values of (3.13). It is also seen that the midpoints of the coexisting densities (dash-dot line) is approximately a linear function of the temperature in the vicinity of the critical point (the straight line is given as a guide to the eye). This corresponds to the so-called law of rectilinear diameters [5] being approximately satisfied.

IV. THE vdW THEORY OF THE SOLID PHASE

For a perfect crystal with lattice sites $\mathbf{r}_j$, we have instead of (3.1)

$$\rho_1^{\mathrm{HS}}(\mathbf{r}) = \sum_{j=1}^{N} \varphi(\mathbf{r} - \mathbf{r}_j), \tag{4.1}$$

where $\varphi(\mathbf{r} - \mathbf{r}_j)$ describes the normalized ($\int d\mathbf{r}\varphi(\mathbf{r}) = 1$) density profile around the site at $\mathbf{r}_j$. Substituting (4.1) into (2.10) yields for (3.2)

$$\Delta f = \frac{1}{2\epsilon N}\sum_{i=1}^{N}\sum_{j=1}^{N}\int d\mathbf{r}\int d\mathbf{r}'\,\varphi(\mathbf{r} - \mathbf{r}_i) \times\varphi(\mathbf{r}' - \mathbf{r}_j)\,V_A(|\mathbf{r} - \mathbf{r}'|). \tag{4.2}$$

while f_{HS} is still given in terms of the HS equation of state by (3.4). For the equation of state of the HS solid we will adopt again a very simple expression [cf. (3.6)]. Like in cell theory [6], we will use a free-distance approximation:

$$\frac{\beta p_{\mathrm{HS}}(\rho)}{\rho} = \frac{1}{1 - \delta^{1/3}};\quad \delta < 1, \tag{4.3}$$

so that $V^{1/3}(1 - \delta^{1/3})$ is the average distance over which the HS can freely move in the HS crystal of volume V. We again write $\delta = \rho/\rho_{\mathrm{cp}}$, so that ρ_{cp} is the maximum value of the density ρ for which the crystal can exist, i.e., ρ_{cp} is the density at close packing (cp) of the given lattice structure. Except for the change from free volume to free distance, (4.3) is similar in spirit to (3.6), with ρ_{cp} being the equivalent for the solid of ρ_0 for the fluid. For $\rho \to \rho_{\mathrm{cp}}$, (4.3) implies

$$\frac{\beta p_{\mathrm{HS}}(\rho)}{\rho} = \left[1 - \left(1 - \frac{\rho_{\mathrm{cp}} - \rho}{\rho_{\mathrm{cp}}}\right)^{1/3}\right]^{-1} \simeq \frac{3\rho_{\mathrm{cp}}}{\rho_{\mathrm{cp}} - \rho} \equiv \frac{3}{1 - \delta} \tag{4.4}$$

and we recover the usual free-volume behavior which holds well [2] for HS at high densities [7] (cf. Fig. 3). In the opposite limit $\delta \to 0$, (4.3) exhibits a free-particle behavior [whereas (4.4) does not] so that (3.4) can again be easily integrated when (4.3) is used, yielding

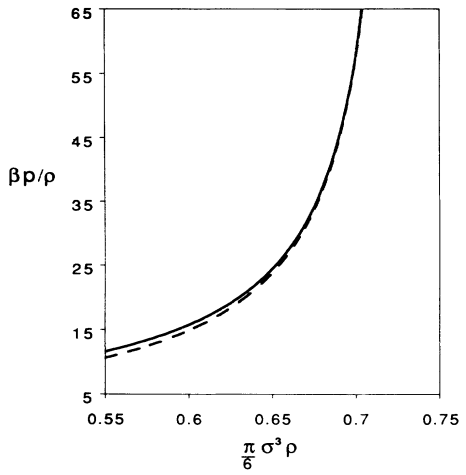

FIG. 3. The HS-compressibility factor $(\beta p/\rho)$ vs the HS-packing fraction $(\pi\rho\sigma^3/6)$ as obtained from the simple Eq. (4.3) (broken line) compared to the fit to the computer simulations of a fcc-HS solid (full line) as proposed by Hall [7].

$$f_{\rm HS} = t[C_s + \ln\delta - 3\ln(1-\delta^{1/3})] \equiv t[C_s - 3\ln(x_1-1)], \tag{4.5}$$

where

$$C_s = \ln(\rho_{\rm cp}\Lambda^3) - 1;\ \delta = \frac{\rho}{\rho_{\rm cp}} = \frac{1}{x_1^3} \tag{4.6}$$

so that C_s is the analog of C_f [cf. (3.10)], while $x_1 = (\rho_{\rm cp}/\rho)^{1/3}$ is the reduced nearest-neighbor distance r_1, i.e., $x_1 = r_1/\sigma$, for a crystal of density ρ and a crystal structure of close packing density $\rho_{\rm cp}$. To proceed with (4.2) we distinguish two cases.

A. $\phi(x)$ is continuous for $x > 1$

In this case, we can take into account the fact that in the HS crystal the particles are strongly localized by approximating the density profile $\varphi(\mathbf{r}-\mathbf{r}_j)$ of (4.1) by a delta function, in which case (4.2) simply yields

$$\Delta f = \frac{1}{2\epsilon N}\sum_{i=1}^{N}\sum_{j=1}^{N} V_A(|\mathbf{r}_j - \mathbf{r}_i|) = -\frac{1}{2}\sum_{j=1}^{N}\phi(x_j), \tag{4.7}$$

where we have used (2.12) and taken into account that in a perfect crystal all the sites are equivalent in order to reduce the double sum of (4.7) to a simple sum over the sites j with $x_j = |\mathbf{r}_j - \mathbf{r}_i|/\sigma$ being the reduced distance of site j to an arbitrary site i taken as origin ($\mathbf{r}_i = 0$). At this stage it may be useful to notice the similarity of (4.7) with (3.3). Indeed, if we write

$$\Delta f = \frac{1}{2\epsilon}\int d\mathbf{r}\, V_A(r)\,\bar\rho(\mathbf{r}), \tag{4.8}$$

where $\bar\rho(\mathbf{r})$ is now the distribution of sites, then for the crystal we have $\bar\rho(\mathbf{r}) = \sum_j \delta(\mathbf{r}-\mathbf{r}_j)$ and (4.8) will restore (4.7) while for a fluid we have $\bar\rho(\mathbf{r}) = \rho$ and (4.8) restores (3.3).

To proceed we can rewrite the lattice sum (4.7) in terms of a sum over spherical shells of sites centered around the site at the origin, with the jth shell containing n_j sites:

$$\Delta f = -\frac{1}{2}\sum_{j}^{\rm sites}\phi(x_j) = -\frac{1}{2}\sum_{j}^{\rm shells} n_j\,\phi(x_j), \tag{4.9}$$

which is similar to the approximation already used elsewhere [8] for a purely repulsive potential. Notice that the site (shell) at the origin, $x_0 = 0$ and $n_0 = 1$, does not contribute to (4.9) because $\phi(0)$ is a constant which can always be put equal to zero, since in the presence of a HS repulsion $\phi(x)$ need to be defined only for $x \geq 1$ [cf. (2.12)]. Ordering the remaining shells by increasing radii $(x_1 < x_2 < x_3 \cdots)$ we can for a decreasing $\phi(x)$ only keep the dominant term:

$$\Delta f = -\frac{1}{2}\,n_1\,\phi(x_1), \tag{4.10}$$

where n_1 is the number of nearest neighbors and x_1 the reduced nearest-neighbor distance of the given crystal structure as it appears already in (4.5,4.6). The present vdW theory, (4.5) and (4.10), yields, thus,

$$f = t[C_s - 3\ln(x_1-1)] - \frac{1}{2}n_1\phi(x_1), \tag{4.11}$$

$$\bar\mu = t\left[C_s - 3\ln(x_1-1) + \frac{x_1}{x_1-1}\right] - \frac{1}{2}n_1\phi(x_1) + \frac{1}{6}n_1x_1\phi'(x_1), \tag{4.12}$$

$$\frac{\bar p}{\rho_{\rm cp}\sigma^3} = \frac{t}{x_1^2(x_1-1)} + \frac{n_1\phi'(x_1)}{6x_1^2}, \tag{4.13}$$

which are the equivalents for the solid of (3.7–3.9). As usual, $\phi'(x) = d\phi(x)/dx$, etc. Since $\phi(x) > 0$, (4.11) implies a vdW loop for the solid. From (4.13) we obtain for the solid(S_1)-solid(S_2) critical point, using (3.12)

$$\frac{3x_1^c - 2}{(x_1^c-1)^2} = \frac{n_1}{6t_c}[x_1^c\phi''(x_1^c) - 2\phi'(x_1^c)], \tag{4.14}$$

$$\frac{2(2x_1^c-1)}{(x_1^c-1)(3x_1^c-2)} = \frac{2\phi'(x_1^c) - (x_1^c)^2\phi'''(x_1^c)}{x_1^c\phi''(x_1^c) - 2\phi'(x_1^c)}, \tag{4.15}$$

while the solid(S_1)-solid(S_2) coexistence curve can be obtained from (4.12,4.13) using (3.14), yielding

$$\frac{u_2^2}{u_1-1} - \frac{u_1^2}{u_2-1} = \frac{n_1}{6t}[u_1^2\phi'(u_2) - u_2^2\phi'(u_1)], \tag{4.16a}$$

$$u_2(u_1-1) - u_1(u_2-1) + 3(u_1-1)(u_2-1)\ln\left(\frac{u_1-1}{u_2-1}\right) = [u_2^2(u_2-1) - u_1^2(u_1-1)] \times \left[\frac{u_1\phi'(u_1) - u_2\phi'(u_2) - 3[\phi(u_1)+\phi(u_2)]}{u_1^2\phi'(u_2) - u_2^2\phi'(u_1)}\right], \tag{4.16b}$$

where u_1 and u_2 denote, respectively, the value of x_1 for S_1 and S_2. We will assume $u_1 < u_2$ so that S_1 is the high-density solid and S_2 the low-density solid. As an illustration, we will consider now the case of an IP attraction, $\phi(x) = 1/x^n$ (cf. Fig. 1). Equations (4.14,4.15) reduce to

$$\frac{3x_1^c - 2}{(x_1^c - 1)^2} = \frac{n_1 n(n+3)}{6t_c (x_1^c)^{n+1}}, \tag{4.17}$$

$$\frac{2(2x_1^c - 1)}{(x_1^c - 1)(3x_1^c - 2)} = n. \tag{4.18}$$

From (4.18), one easily finds x_1^c as

$$x_1^c = \frac{\sqrt{n^2 + 16n + 16} + 5n + 4}{6n} \simeq 1 + \frac{2}{n} - \frac{4}{n^2} + \cdots \tag{4.19}$$

which, on substitution of (4.19) into (4.17), yields for the critical temperature t_c

$$t_c = \frac{2n_1}{3e^2}\left(1 - \frac{3}{n} + \cdots\right) \tag{4.20}$$

to dominant order in $1/n$. Substituting (4.19) and (4.20) into (4.13) yields for the critical pressure $p_c/\epsilon\rho_{cp} = nt_c/4$, for $n >> 1$. The exact behavior of x_1^c and t_c vs $1/n$ is shown in Fig. 4. From (4.16) one can also obtain the coexistence curve; a few examples are shown in Fig. 5. Notice that here there is no law of corresponding states, nor of rectilinear diameters. Also, when $1/n$ decreases, ρ_c and t_c increase towards an upper limit, respectively, ρ_{cp} and $2n_1/3e^2$, whereas for the fluid ρ_c remains constant while t_c decreases towards zero [cf. (3.13)].

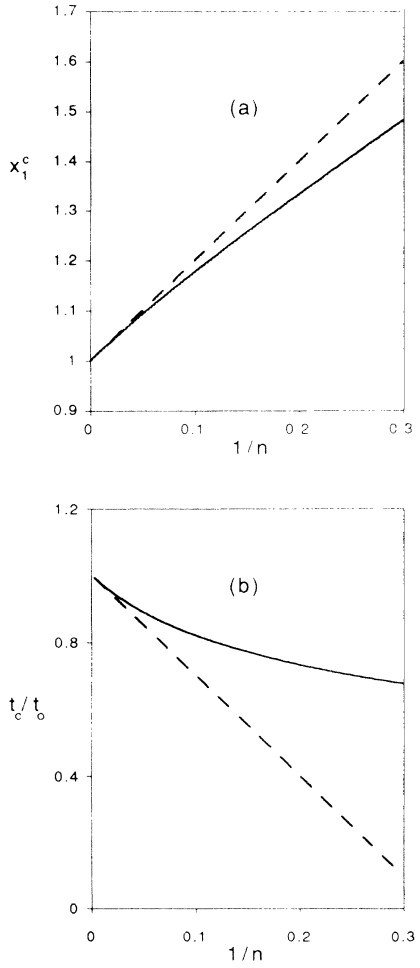

FIG. 4. The critical point values of (a) the nearest-neighbor distance (x_1^c) and (b) reduced temperature (t_c) for the isostructural solid-solid transition predicted by (4.11) for an IP attraction (2.14) of index n. The full lines correspond to the exact results obtained from (4.17,4.18) and the broken lines to the asymptotic expansions (4.19,4.20). Here $t_0 = 2n_1/3e^2$, with n_1 the number of nearest neighbors and hence $t_0 \simeq 1.08$ for a fcc structure ($n_1 = 12$).

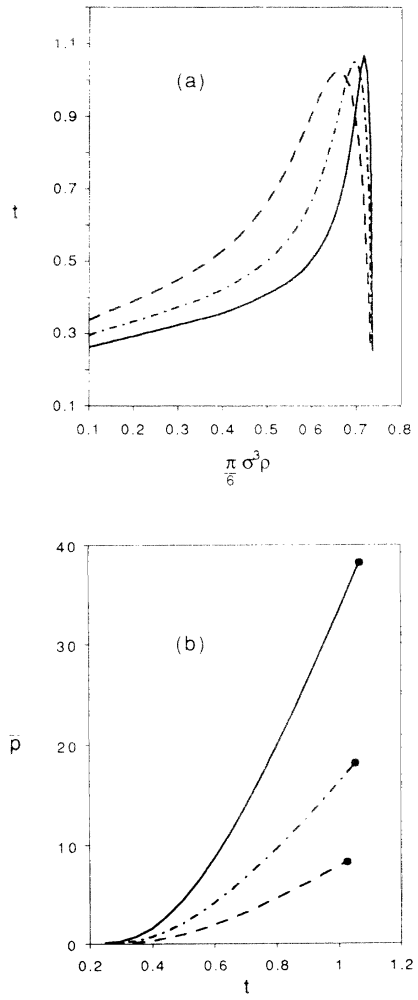

FIG. 5. A few examples of coexistence curves in the (a) temperature(t)-density($\bar{\rho}$) and (b) the pressure($\bar{p}$)-temperature(t) planes for the fcc isostructural solid(S_1)-solid(S_2) transition as obtained from (4.16) for an IP attraction of index $n = 50$ (dashed line), 100 (dash dot line), and 200 (full line).

B. $\phi(x)$ is discontinuous for $x > 1$

In this case, we cannot use (4.7) because the discontinuity of $\phi(x)$ will be transferred to the free energy f, which is not allowed by thermodynamics. To cope with this case we have to maintain finite the width of the density profile $\varphi(\mathbf{r}-\mathbf{r}_j)$ of (4.1,4.2). We observe that it has been shown [9] that in the HS crystal $\varphi(\mathbf{r})$ is very nearly Gaussian and we can hence approximate it as

$$\varphi(\mathbf{r}) \simeq \left(\frac{\alpha}{\pi}\right)^{3/2} e^{-\alpha r^2} \equiv \varphi_\alpha(r). \tag{4.21}$$

Substituting (4.21) into (4.2) and taking into account that the convolution of two Gaussians yields a Gaussian, we obtain for (4.2):

$$\Delta f = \frac{1}{2\epsilon} \sum_j^{\text{shells}} n_j \int d\mathbf{r}\, V_A(r)\, \varphi_{\alpha/2}(|\mathbf{r}-\mathbf{r}_j|) \tag{4.22}$$

or comparing with (4.8), $\bar{\rho}(\mathbf{r}) = \sum_j \varphi_{\alpha/2}(|\mathbf{r}-\mathbf{r}_j|)$, where in (4.22) we have put a site at the origin and sum over the spherical shells of sites around the one at the origin. Using (2.12) and (4.21) we can reduce (4.22) to

$$\Delta f = -\frac{1}{2} \sum_j^{\text{shells}} n_j \left(\frac{\alpha\sigma^2}{2\pi x_j^2}\right)^{1/2} \int_1^\infty dx\, x\phi(x) \times \left[e^{-\alpha\sigma^2(x-x_j)^2/2} - e^{-\alpha\sigma^2(x+x_j)^2/2}\right] \tag{4.23}$$

where, as above, n_j denotes the number of sites in the jth shell located a distance, $x_j = |\mathbf{r}_j|/\sigma$, from the site at the origin. Since in a solid the Gaussians of (4.21) are very narrow, i.e., $\alpha\sigma^2$ is very large, we again keep only the dominant contribution to (4.23). We find that the contribution to (4.23) from the site at the origin ($n_0 = 1$, $x_0 = 0$) is exponentially small, while ordering the shells as before ($x_1 < x_2 < x_3 \cdots$) we find that (4.23) is again dominated by the shell of nearest neighbors, i.e.,

$$\Delta f \simeq -\frac{1}{2} n_1 \left(\frac{\alpha\sigma^2}{2\pi x_1^2}\right)^{1/2} \int_1^\infty dx\, x\phi(x) e^{-\alpha\sigma^2(x-x_1)^2/2}, \tag{4.24}$$

where we took moreover into account that in (4.23) the contribution of the second exponential is always small with respect to the first. We will illustrate here the use of (4.24) for the case of the SW potential of (2.13). For this case (4.24) reduces to

$$\Delta f = -\frac{1}{2} n_1 \left(\frac{\alpha\sigma^2}{2\pi x_1^2}\right)^{1/2} \int_1^{1+\gamma} dx\, x e^{-\alpha\sigma^2(x-x_1)^2/2} = -\frac{1}{4} n_1 \left[\operatorname{erf} y_1 - \operatorname{erf} y_2 + \left(\frac{2}{\pi\alpha\sigma^2 x_1^2}\right)^{1/2} (e^{-y_1^2} - e^{-y_2^2})\right], \tag{4.25}$$

where erf denotes the error function [$\operatorname{erf} x = (2/\sqrt{\pi}) \int_0^x dt\, e^{-t^2}$], while y_1 and y_2 are given by

$$y_1 = \left(\frac{\alpha\sigma^2}{2}\right)^{1/2} (x_1 - 1); \qquad y_2 = \left(\frac{\alpha\sigma^2}{2}\right)^{1/2} [x_1 - (1+\gamma)]. \tag{4.26}$$

To proceed, we eliminate the inverse width of the Gaussians, $\alpha\sigma^2$, in terms of the Lindemann ratio, $L = \sqrt{\langle r^2\rangle}/r_1$. For the Gaussian (4.21) we have, $\langle r^2\rangle = 3/2\alpha$ and hence $L^2 = 3/2x_1^2\alpha\sigma^2$. This allows us to rewrite (4.26) as

$$y_1 = \frac{\sqrt{3}}{2L}\left[\frac{x_1-1}{x_1}\right]; \quad y_2 = \frac{\sqrt{3}}{2L}\left[\frac{x_1-(1+\gamma)}{x_1}\right]. \tag{4.27}$$

By definition L vanishes at close packing ($\rho = \rho_{cp}$ or $x_1 = 1$), while it has a finite value of the order of 0.15 at

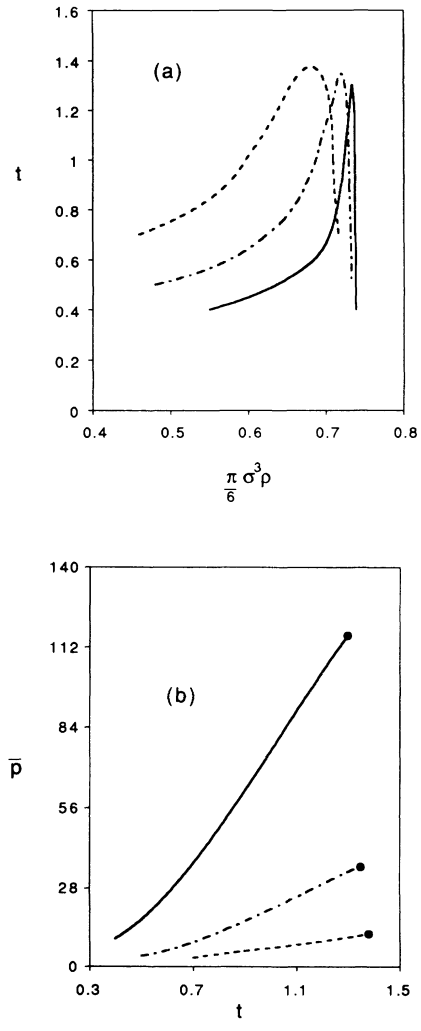

FIG. 6. The same as in Fig. 5 but for a SW attraction of range $\gamma = 0.003$ (full line), 0.01 (dash dot line), 0.03 (dashed line) as obtained from (4.29,4.30) with $L_0 = 0.477$ (see text).

melting [2]. For HS it was found elsewhere [10] that L varies approximately linearly with the density in between these two limits. We will write, hence,

$$L = L_m \left[\frac{1-\eta}{1-\eta_m}\right] = L_0 \left[\frac{x_1^3 - 1}{x_1^3}\right], \tag{4.28}$$

where $L_0 = L_m/(1-\eta_m)$ and L_m and η_m are, respectively, the value of L and η at melting of the HS crystal. Combining (4.25–4.28) with (4.5) we obtain, thus, finally for (3.2):

$$f = t[C_s - 3\ln(x_1 - 1)] - \frac{1}{4}n_1 \left[\operatorname{erf} y_1 - \operatorname{erf} y_2 + \frac{x_1 - 1}{\sqrt{\pi} x_1 y_1}(e^{-y_1^2} - e^{-y_2^2})\right], \tag{4.29}$$

with

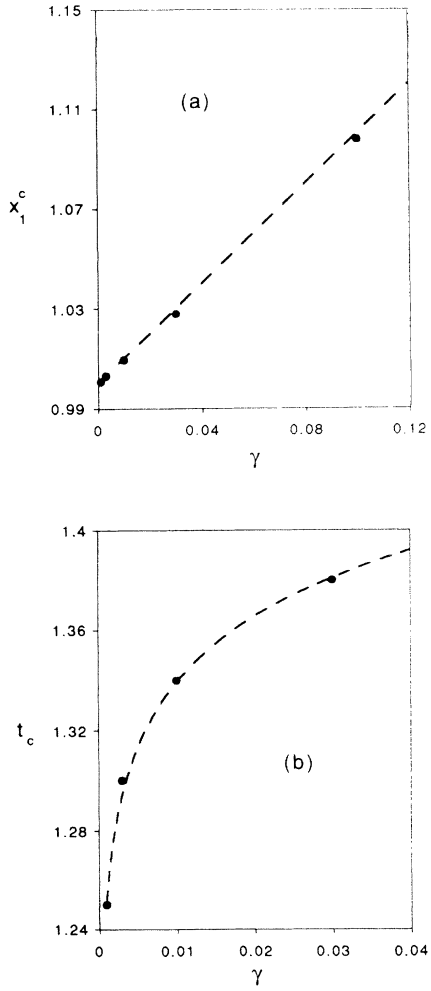

FIG. 7. The same as in Fig. 4 but for a SW attraction of range $\gamma = 0.001, 0.003, 0.01, 0.03, 0.1$ (dots). The broken lines correspond to the small-γ fits: $x_1^c \simeq 1 + \gamma$ and $t_c \simeq 1.514 + 0.038 \ln\gamma$. Notice that while our values of x_1^c correspond closely to those of [3], our values of t_c do not seem to have a small-γ limit.

$$y_0 = \frac{\sqrt{3}}{2L_0};\quad y_1 = y_0 \left[\frac{x_1^2}{x_1^2 + x_1 + 1}\right];$$
$$y_2 = y_1 \left[1 - \frac{\gamma}{x_1 - 1}\right], \tag{4.30}$$

where y_0 is a constant to be borrowed from the HS freezing theory ($y_0 \simeq 1.81$, see Sec. V). Although the SW potential is simpler than the IP potential, the resulting vdW free energy (4.29) is more complicated than (4.11). This is due to the fact that the discontinuity of $\phi_{SW}(x)$ at $x = 1 + \gamma$ did prevent us from considering the limit $\alpha \to \infty$, where the density profile $\varphi_\alpha(\mathbf{r})$ becomes a singular δ function. The results obtained from (4.29) are nevertheless very similar to those obtained from (4.11). A few examples are shown in Fig. 6. Notice that the critical density corresponds very closely (see Fig. 7) to the value of x_1 for which y_2 of (4.30) changes sign, i.e., $x_1^c \simeq 1 + \gamma$. Therefore the critical density $\rho_c = \rho_{cp}/(x_1^c)^3$ increases towards the upper limit ρ_{cp} when γ decreases, just as in the IP case. Notice however that the critical temperature t_c of the SW case has a behavior opposite to that of the IP: here t_c decreases when $\gamma \to 0$ (see Fig. 7).

V. PHASE DIAGRAMS IN THE vdW APPROXIMATION

The basic macroscopic effect of the presence of an attraction is, according to the vdW approximation, to produce a vdW loop in the free energy for subcritical temperatures. It is well known that this is the case for the fluid phase, as we recalled in Sec. III, but occurs also for the solid phase, as shown in Sec. IV and in Refs. [3,4]. As is well known, this loop separates the free energy of a given phase into two branches, say a low-density branch and a high-density branch, separated by an unstable part, corresponding to a negative compressibility, where the free-energy curve turns from a convex into a concave curve. Performing Maxwell's double tangent construction on such a loop of f versus $v = 1/\rho\sigma^3$ one finds, at the two points of tangency, the phase of the low-density branch which can coexist at the given temperature with the phase of the high-density branch, i.e., two phases having equal pressure and equal chemical potential. For instance, below the critical temperature of the fluid, the fluid phase (F) will undergo a F_1-F_2 transition resulting in the coexistence (see Sec. III) between a low-density fluid phase (F_1) and a high-density fluid phase (F_2), as is well known from the liquid(F_2)-gas(F_1) transition. Similarly, below the (different) critical temperature of the solid, the solid phase (S) will undergo a S_1-S_2 transition resulting in the coexistence (see Sec. IV) between a high-density (S_1) solid and a solid of the same structure but of a lower density (S_2). This transition was called the expanded (S_2) to condensed (S_1) transition in Ref. [3]. Besides, one can always perform a double tangent construction between the free energy of the fluid and that of the solid. The corresponding fluid-solid transition will be indicated here as F-S, where it is understood that, in

general, we have $F \neq F_1 \neq F_2$ and $S \neq S_1 \neq S_2$. Not all these transitions are thermodynamically stable however. Only those phases are stable which belong to the convex envelope constructed with the aid of the four free-energy branches (F_1, F_2, S_1, S_2) and the three double tangents (F_1-F_2, S_1-S_2, S-F). A closer inspection of the triangles formed by the three double tangents indicates that the competition between the above two vdW loops can only produce three distinct types of phase diagrams (see Fig. 8). Notice also that for $\phi(x)$ expressions more complicated than those considered here there could be more than one vdW loop in the solid free energy but we will not pursue this possibility here and stick to the two cases (2.13,2.14).

Before we can construct the phase diagrams, there remains to fix the relative position of the free energies. As seen from Sec. III, the free energy of the HS fluid depends only on the scaled density variable, ρ/ρ_0, where ρ_0 fixes the stability limit ($0 < \rho < \rho_0$) of the fluid. Similarly, in Sec. IV we show that the free energy of the HS solid depends on the scaled density variable, ρ/ρ_{cp}, where ρ_{cp} fixes the stability limit of the solid ($0 < \rho < \rho_{cp}$). When, as before, each phase is taken separately the value of the two constants, ρ_0 and ρ_{cp}, is immaterial except for the obvious geometric restrictions, $\pi\sigma^3\rho_0/6 < 1$, $\pi\sigma^3\rho_{cp}/6 < 1$. When constructing the phase diagram the two phases are required and the relative free energy depends then on $\ln(\rho_0/\rho_{cp})$, which requires that we first fix the value of these constants. From the derivation in Sec. IV it is obvious that ρ_{cp} is determined by the value of ρ at close packing of the crystal structure considered. For example, for a face centered cubic or fcc structure we have $\rho_{cp}\sigma^3 = \sqrt{2}$ and $n_1 = 12$. As to ρ_0, the only restriction is $0.494 < \pi\rho_0\sigma^3/6 < 1$ since we know from the computer simulations [2] that the HS fluid is stable at least up to the freezing density $\pi\rho_f\sigma^3/6 = 0.494$. Here we will fix ρ_0 in such a manner that the HS free energies, in the absence of any attraction [$\phi(x) = 0$], cross at $\pi\rho\sigma^3/6 = 0.515$ in agreement with the results obtained elsewhere [10]. This is seen to imply $\pi\rho_0\sigma^3/6 = 0.5157$, i.e., the HS fluid becomes unstable shortly after it becomes metastable with respect to the fcc HS solid. When improved HS equations of state are used, the HS free energies will automatically cross at this density but notice that one cannot simply improve the equation of state of one phase, and keep a simple free-volume approximation for the other phase because some of these combinations are void of HS free-energy crossing. In order to keep the proper HS free-energy crossing, one usually will have to improve both the description of the fluid and of the solid. As long as the proper HS crossing is guaranteed the results are qualitatively similar whatever the HS equations of state used. Here we have introduced an ρ_0 parameter in the description of the HS fluid in order to be able to use very simple (free-volume) equations of state, just as in the original vdW theory, and then chosen the value of $\pi\rho_0\sigma^3/6$ to be approximately 0.52 so as to secure the proper HS free energy crossing. Once these constants (ρ_0, ρ_{cp}) are fixed, the phase diagram of the system depends only on the range of the attractions, i.e., the value of γ (SW) or $1/n$ (IP) in (2.13,2.14). Notice that in the particular case of

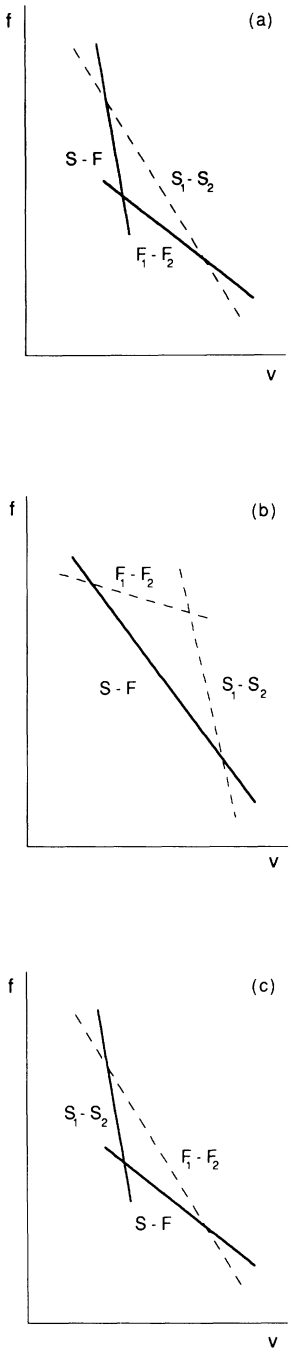

FIG. 8. To construct the convex envelope of f vs v we consider the 12 possible triangles formed by the three double tangents (F_1-F_2, S_1-S_2, and S-F) of negative slope (positive pressure). For only six triangles will the S-F double tangent always belong to the convex envelope. For only three of these six triangles do we have that the pressure of the coexisting solids is larger than the pressure of the coexisting fluids . The latter three triangles generate (when changing the temperature) the three types of phase diagrams found. An example of each of these three situations is shown in the figure (the double tangents belonging to the convex envelope are the full lines while the dashed lines correspond to metastable coexistences). The three cases shown belong to attractions of long (a), intermediate (b), and short (c) range.

the discontinuous SW attraction we also need the value of L_0 [cf. (4.30)]. For the fcc-HS crystal, we have (see [2]) $L_m = 0.126$ and $\eta_m = 0.545 \times (3\sqrt{2}/\pi) \simeq 0.736$, and hence $L_0 \simeq 0.477$.

We now consider, as an illustration, the calculation of the phase diagrams, within the present vdW approximation, for the particular case of a SW attraction (2.13), since this is a case for which simulations are available [3]. The two phases considered are, a fluid phase described by the free energy (3.7) and a fcc crystal described by the free energy (4.29). For a fcc structure, we have $n_1 = 12$ and $\pi\rho_{cp}\sigma^3/6 = \pi/3\sqrt{2}$. As explained above, the two inputs are $\pi\rho_0\sigma^3/6 = 0.5157$ for the fluid and $L_0 = 0.477$ for the solid. Using the reduced temperature, $t = k_BT/\epsilon$, and the reduced pressure, $\bar{p} = p\sigma^3/\epsilon$, the phase diagrams will depend only on γ, i.e., the range of the SW-attraction relative to the HS repulsion. In agreement with the other, more rigorous, calculations of Refs. [3,4] and with the general argument above, we find three different types of phase diagrams. For large γ values we find the usual type of phase diagram with a F_1-F_2 critical point and a F_1-F_2-S triple point. Lowering γ we find that for, $0.3 > \gamma > 0.2$, there is a first crossover (say for $\gamma \simeq 0.25$; see Fig. 9) to a phase diagram without the high-density (liquid) F_2 phase. For still lower γ values, we find, for $0.02 > \gamma > 0.01$, a second crossover (say for $\gamma \simeq 0.015$; see Fig. 10) to a phase diagram with a S_1-S_2 critical point and a S_1-S_2-F triple point. The first threshold, $\gamma \simeq 0.25$ for the disappearance of the dense fluid (liquid) phase, corresponds to the F_1-F_2 coexistence curve "disappearing" into the inside of the F-S coexistence region, as a result of the lowering of the F_1-F_2 critical temperature when lowering γ. The second threshold, $\gamma \simeq 0.015$ for the appearance of the expanded solid, corresponds to the S_1-S_2 coexistence curve "emerging" from the interior of the F-S coexistence curve as a result of the increase of the S_1-S_2 critical density when lowering γ. There is thus a remarkable solid-fluid symmetry with respect to the low-high values of γ. These vdW results are in complete qualitative agreement, and to some extent also in quantitative agreement, with the more exact results of Refs. [3,4]. Indeed, the coexistence

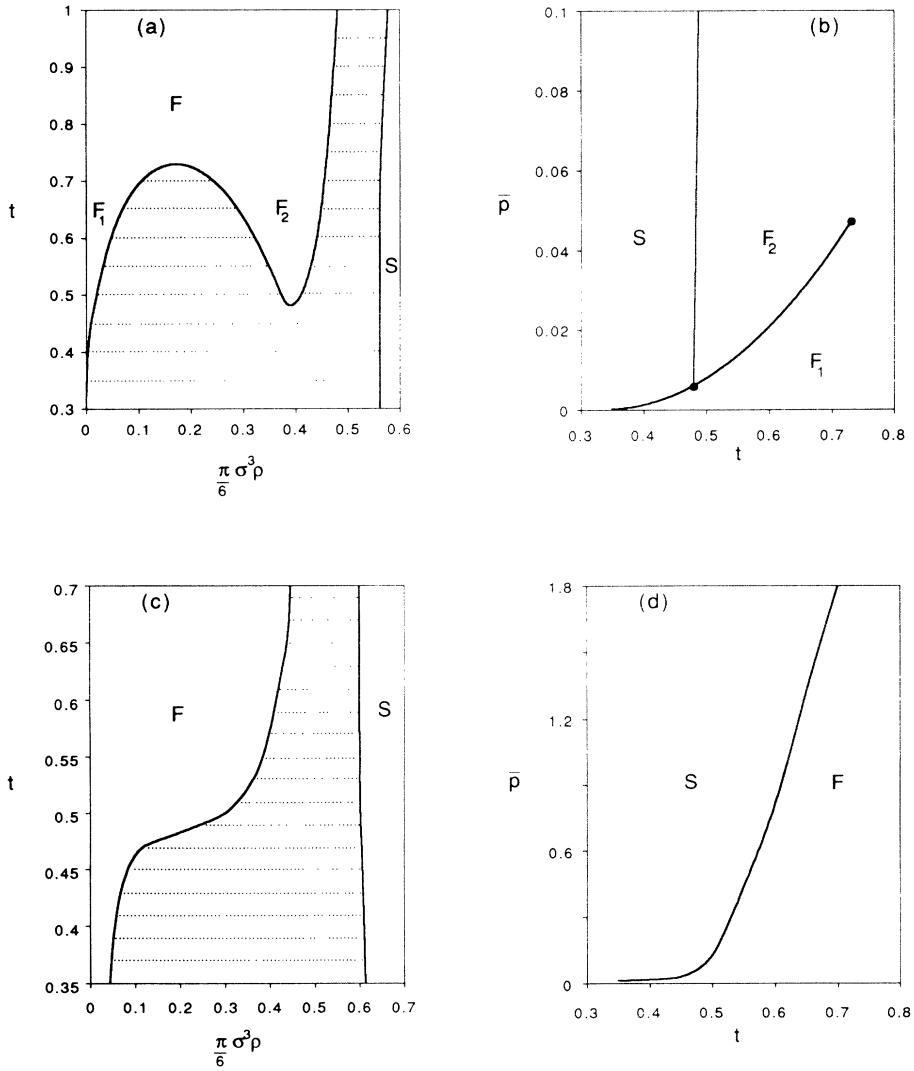

FIG. 9. Phase diagrams in the temperature(t)-density($\bar{\rho}$) and the pressure($\bar{p}$)-temperature(t) planes for the case of a SW attraction of range γ. Shown are two cases bracketing the threshold ($\gamma \simeq 0.25$) for the disappearance of the high-density fluid (or liquid) phase. [$\gamma = 0.3$ for (a), (b) and $\gamma = 0.2$ for (c), (d)].

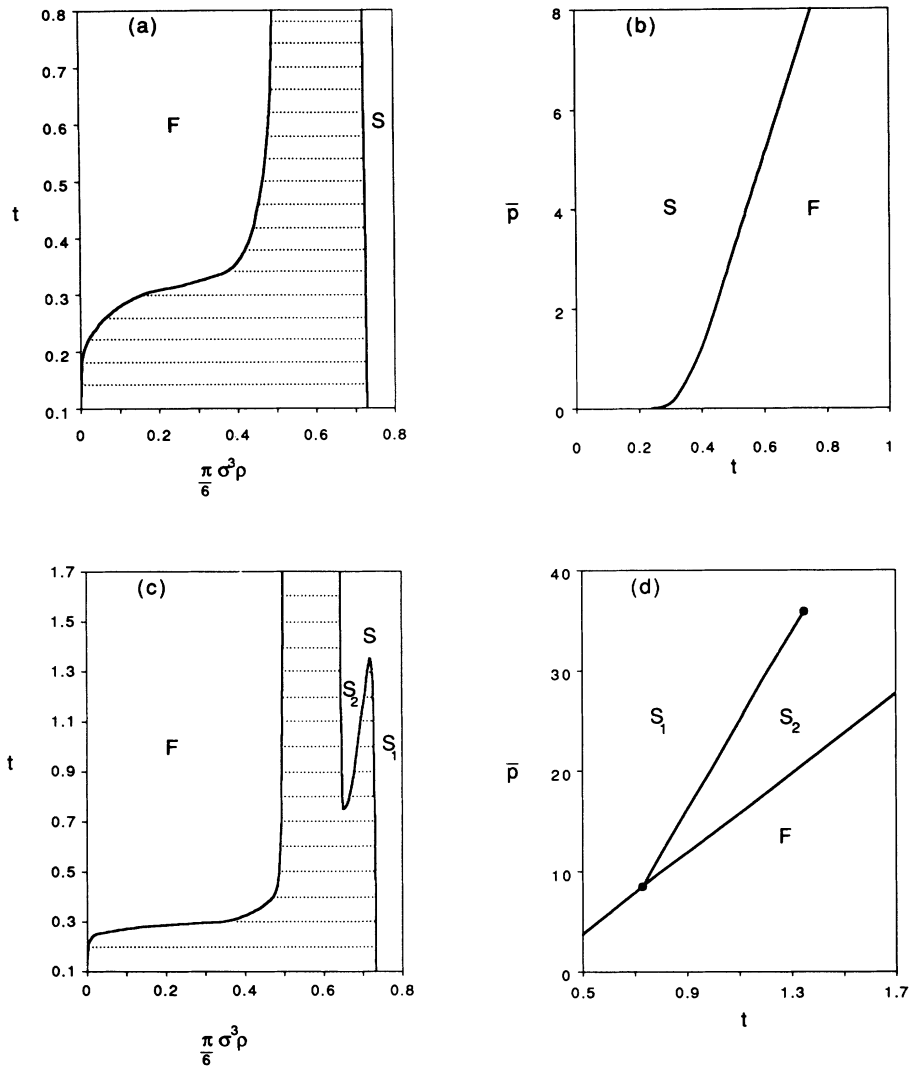

FIG. 10. The same as in Fig. 9 but for two values of γ bracketing the threshold ($\gamma \simeq 0.015$) for the appearance of the low-density (or expanded) solid phase. [$\gamma = 0.02$ for (a), (b) and $\gamma = 0.01$ for (c), (d)].

curves found here are very similar to those of [3,4] while the thresholds and critical points are also comparable. Similar results are obtained for the IP attraction: here, the threshold values of n are, $7 < n < 8$, for the first threshold and, $90 < n < 100$, for the second threshold.

VI. CONCLUSIONS

We have shown that the recent results [3,4] concerning the effect of the range of the attractions relative to the range of the repulsions of a simple fluid on its phase diagram can be semiquantitatively understood in terms of the competition of the standard vdW theory of the fluid phase with the alternative [12] but equally simple vdW theory of the solid-phase introduced above. In particular, we have shown that this competition leads to three different types of phase diagrams with a remarkable solid-fluid symmetry. For the case of a square-well attraction of range γ it was shown, in agreement with other findings [11,3,4], that the liquid phase disappears as a stable phase for γ values below $\gamma \simeq 0.25$, while a new stable solid phase appears for γ values below $\gamma \simeq 0.015$. As discussed elsewhere [13,3,4] such small values of γ can perhaps be realized in well-prepared colloidal dispersions where the depletion forces due to the added polymer will account for the attraction between the colloidal particles allowing for a "simple fluid" description to be used for this otherwise complex system.

ACKNOWLEDGMENTS

C. F. Tejero acknowledges the DGICYT (Spain) (PB91-0378) and M. Baus the FNRS (Belgium) and the Association Euratom-Etat Belge. M. Baus gratefully acknowledges valuable discussions with H. N. W. Lekkerkerker about the interest of this study for the phase behavior of colloidal dispersions.

[1] See, e.g., L. D. Landau and E. M. Lifshitz, *Statistical Physics*, 3rd ed. (Pergamon Press, Oxford, 1989), Sec. 76.
[2] J. P. Hansen and I. R. McDonald, *Theory of Simple Liquids*, 1st ed. (Academic Press, London, 1976).
[3] P. Bolhuis and D. Frenkel, Phys. Rev. Lett. **72**, 2211 (1994).
[4] C. F. Tejero, A. Daanoun, H. N. W. Lekkerkerker, and M. Baus, Phys. Rev. Lett. **73**, 752 (1994).
[5] J. S. Rowlinson, *Liquids and Liquid Mixtures* (Butterworths, London, 1959), p. 90.
[6] T. M. Reed and K. E. Gubbins, *Applied Statistical Mechanics* (Mc Graw-Hill, Tokyo, 1973), p. 282.
[7] R. Hall, J. Chem. Phys. **57**, 2252 (1972).
[8] J. F. Lutsko and M. Baus, J. Phys. Condens. Matter **3**, 6547 (1991).
[9] R. Ohnesorge, H. Löwen, and H. Wagner, Europhysics Lett. **22**, 245 (1993).
[10] J. F Lutsko and M. Baus, Phys. Rev. A **41**, 6647 (1990).
[11] A. P. Gast, C. K. Hall, and W. B. Russel, J. Colloid Interface Sci. **96**, 251 (1983).
[12] An alternative vdW theory for the solid can be found in D. A. Young, J. Chem. Phys. **98**, 9819 (1993). The latter vdW theory is inspired by the fluid-phase theory and hence treats the cohesive energy as a phenomenological constant whereas here it is given explicitly in terms of the attractive potential $\phi(x)$ by (4.10).
[13] For a recent review see, e.g., H. N. W. Lekkerkerker, J. K. G. Dhont, H. Verduin, C. Smits, and J. S. van Duijneveldt, Physica A (to be published).